Magnetic structures of the iridium-based double perovskites Pr2NiIrO6 and Nd2NiIrO6 reinvestigated using neutron diffraction

C. Ritter, S. Sharma, and D. T. Adroja

Published version information

Citation: C Ritter, S Sharma and DT Adroja. Magnetic structures of the iridium-based double perovskites Pr2NiIrO6 and Nd2NiIrO6 reinvestigated using neutron diffraction. Phys Rev Materials 6, no. 8 (2022): 084405.

DOI: 10.1103/PhysRevMaterials.6.084405

Magnetic structures of the iridium-based double perovskites Pr_2NiIrO_6 and Nd_2NiIrO_6 reinvestigated using neutron diffraction

C. Ritter [1,*] S. Sharma [2,†] and D. T. Adroja [3,4]

[1]*Institut Laue-Langevin, 71 Avenue des Martyrs, CS 20156, 38042 Grenoble, France*
[2]*National High Magnetic Field Laboratory, Tallahassee, Florida 32310, USA*
[3]*ISIS facility, Rutherford Appleton Laboratory, Chilton Oxon OX11 0QX, United Kingdom*
[4]*Highly Correlated Matter Research Group, Physics Department, University of Johannesburg, Auckland Park 2006, South Africa*

(Received 26 April 2022; revised 9 June 2022; accepted 5 July 2022; published 5 August 2022)

The magnetic structures of the double perovskites Pr_2NiIrO_6 and Nd_2NiIrO_6 have been reinvestigated using high-intensity neutron power diffraction and compared with previously published results by Kayser *et al.* [Acta Mater. **207**, 116684 (2021)] and Ferreira *et al.* [Phys. Rev. Mat. **5**, 064408 (2021)]. The strongly enhanced statistics of neutron diffraction data used in this paper help us to disentangle the complicated coexisting magnetic orderings of the three sublattices in Pr_2NiIrO_6 and Nd_2NiIrO_6. A mainly ferrimagnetic ordering with additional antiferromagnetic components with propagation vector $k = 0$ has been confirmed in both Pr_2NiIrO_6 and Nd_2NiIrO_6 compounds below the magnetic orderings $T_C = 110$ and 120 K, respectively. Nd_2NiIrO_6 further undergoes a second magnetic transition from a ferrimagnet with $k = 0$ to an antiferromagnetic state with $k = (\frac{1}{2}, \frac{1}{2}, 0)$ below $T_N = 15$ K. A partial persistence of the $k = 0$ type order leads, however, to a coexistence of both magnetic phases below T_N not detected previously. The coexistence points to the energies of the magnetic ground states being very similar. Ordered magnetic moments of Ir^{4+} amounting at 1.5 K to $\sim 0.6\,\mu_B$ in Pr_2NiIrO_6 and $0.4\,\mu_B$ in Nd_2NiIrO_6 are clearly detected and are compared with the expected value for the $J_{\text{eff}} = \frac{1}{2}$ model.

DOI: 10.1103/PhysRevMaterials.6.084405

I. INTRODUCTION

Double perovskites of type $A_2BB'O_6$ (A = divalent cation and B and B' = transition metals) adopting the ordered rock-salt type structure have been playgrounds to study very different physical phenomena for many years. The archetypical compound Sr_2FeMoO_6 became famous for its high spin polarization at the Fermi level leading to a half-metallic character [1]. It was one of a long series of compounds where the ability of this structure to accommodate very different types of cations on the A, B, and B' sites was exploited to study double exchange and superexchange interactions between the two types of B sites [2]. With the hope to create exploitable tunneling magnetoresistance at high temperatures, the combination of various elements was tested to increase the magnetic ordering temperature [3–5]. The effects of band filling and structural distortions were studied, and the necessity to avoid any significant antisite disorder to optimize the sought-for physical properties led quickly to the result that charge and ionic size differences between B and B' cations strongly determine the degree of order [6–8]. The half-metallic character found in ferrimagnetic Sr_2FeMoO_6 can be exploited to create magnetic tunnel junctions [2], but the presence of many different phenomena such as phase separation [9,10], metal-insulator transitions [11], large magnetoresistance [12], or the recent discovery of octupolar order [13] make the class of double perovskites highly interesting in general.

Apart from the classical double perovskites, where A is divalent and nonmagnetic, the extraordinary capability of this structure type to host different types of cations leads to the existence of $R_2BB'O_6$ compounds, where R = lanthanide [14], adding a third magnetic site or even $Mn_2BB'O_6$ [15,16], where the relatively large ionic size of the high spin Mn^{2+} ion can open the A site for its implantation under high-pressure conditions and allows the occupation of the cation sites exclusively by transition metals. This adds further complexity to the magnetic interactions and can lead, e.g., to the occurrence of several magnetic transitions at different temperatures [17]. Lately, even the formation of double-double perovskites $AA'BB'O_6$ was reported, where not only the B sites but as well the A sites are ordered [18].

The splitting of the d bands of transition metal cations by an octahedral crystal electric field into e_g and t_{2g} levels is normally adequate to describe the electronic state if the spin-orbit coupling (SOC) remains low. This is, however, only the situation for 3d elements, while for 4d and especially for 5d elements, the reduction of the Coulomb interaction together with the increase of the SOC can lead to a strong modification of the electronic band structure. Transition metal oxides based on the 5d element iridium have lately become the subject of strong research activity as a further splitting of the low-lying t_{2g} bands into $J_{\text{eff}} = \frac{1}{2}$ and $\frac{3}{2}$ bands can exist as originally described by Kim *et al.* [19] for Sr_2IrO_4. Completely different physics as exemplified by the Weyl semimetals [20], topological Mott insulators [19], or the search for the Kitaev quantum

*ritter@ill.fr
†phy.shivanisharma@gmail.com

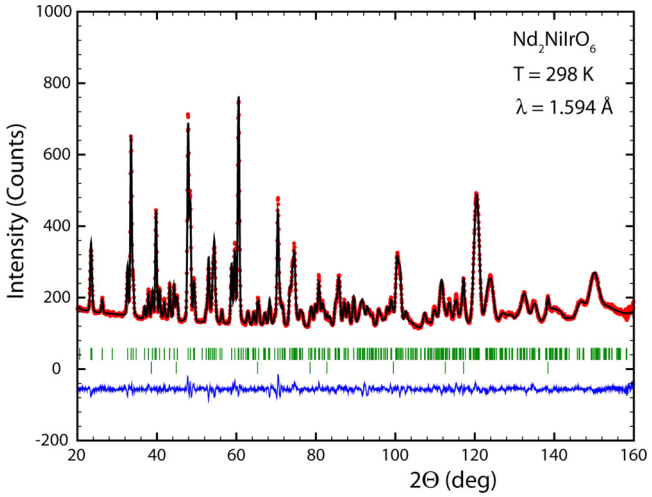

FIG. 1. Refinement of the high-resolution neutron powder diffraction (NPD) data of Nd_2NiIrO_6 at room temperature (RT). Observed (dots, red), calculated (line, black), and difference pattern (line, blue). The tick marks indicate the calculated position of the Bragg reflections of the main phase (upper row) and of the Pt impurity phase (lower row).

spin liquid [21] is strongly based on iridium-containing compounds. The splitting of the t_{2g} bands by strong SOC should lead in Ir^{4+} ($5d^5$)-containing compounds to a magnetic moment of 1 μ_B corresponding to the $J_{\text{eff}} = \frac{1}{2}$ electronic state. The strongly reduced magnetic moment of Ir in the pyrochlore $Nd_2Ir_2O_7$ [22] seems to contradict the prediction for the $J_{\text{eff}} = \frac{1}{2}$ state but was interpreted as resulting from a strong hybridization between the Ir $5d$ and O $2p$ orbitals [23,24]. The often-found reduction of the magnetic moment size together with the strong neutron absorption of Ir makes, however, the determination of the magnetic ordered state of Ir by neutron diffraction difficult. For the double perovskites containing Ir which were studied using neutron diffraction, namely, La_2ZnIrO_6, La_2MgIrO_6 [25], and Nd_2ZnIrO_6 [26], the determination of the Ir magnetic state was therefore not successful, and only a very recent study using highest flux neutron diffraction allowed us to determine the magnetic order and the moment values for La_2ZnIrO_6 and Nd_2ZnIrO_6 [27]. More information including magnetic moment values and spin directions of the Ir sublattice was published for the system R_2NiIrO_6 with R = La, Pr, Nd [28]; however, results presented by a different group [29] were strongly differing. While in Ref. [28] the magnetic propagation vector was assumed to be $k = 0$ for all three compounds, it was given as $k = (\frac{1}{2}, \frac{1}{2}, 0)$ for R = La and, for R = Nd, below a second magnetic transition. Both papers agree on $k = 0$ for Pr_2NiIrO_6 and on the same irreducible representation (IR) describing the magnetic coupling within the unit cell with, however, strongly differing magnetic moment values and spin directions for the three magnetic sublattices of Pr^{3+}, Ni^{2+}, and Ir^{4+}. In a recent study [30], we have shown that the magnetic structure of La_2NiIrO_6 as described by Ferreira *et al.* [29] with $k = (\frac{1}{2}, \frac{1}{2}, 0)$ is correct but represents only one out of several possible models, which can explain the neutron diffraction data. The strongly enhanced statistics used in Ref. [30] allowed us furthermore to ascertain the presence of an ordered moment on the Ir site and its disappearance concomitant with that of the Ni sublattice at $T_N = 74$ K. Here, in this paper, we pursue our efforts to disentangle the complicated coexisting magnetic orderings of the three sublattices in the R = Pr and Nd compounds. By analyzing high statistics neutron powder diffraction (NPD) data, it will be shown that the magnetic structures presented in Ref. [28] are mistaken and that those of Ref. [29] are missing some important details.

TABLE I. BVS error in bond angle averaged, distortion of the IrO_6 octahedra expressed as $\Delta = \frac{1}{6}\sum(d_i - d_0)2/d_o$.

R	Pr		Nd	
T (K)	300	1.5	300	1.5
a (Å)	5.4828(2)	5.4697(2)	5.4475(2)	5.4366(2)
b (Å)	5.6634(2)	5.6718(2)	5.6733(2)	5.6763(3)
c (Å)	7.8062(3)	7.7852(3)	7.7760(2)	7.7585(3)
β(°)	90.0	90.01(2)	90.05(1)	89.99(2)
x_R	0.0162(7)	0.0161(9)	0.0161(4)	0.0140(5)
y_R	0.5586(3)	0.5610(4)	0.5616(2)	0.5627(3)
z_R	0.754(3)	0.759(2)	0.751(2)	0.752(2)
x_{O1}	0.0948(4)	0.0974(5)	0.0976(4)	0.0994(5)
y_{O1}	0.0244(5)	0.0261(6)	0.0268(4)	0.0280(5)
z_{O1}	0.248(3)	0.260(1)	0.252(2)	0.241(1)
x_{O2}	0.199(2)	0.201(2)	0.200(2)	0.196(2)
y_{O2}	0.290(1)	0.2865(8)	0.296(1)	0.300(2)
z_{O2}	−0.051(1)	−0.0530(8)	−0.054(1)	−0.0590(7)
x_{O3}	0.198(2)	0.197(2)	0.194(2)	0.196(2)
y_{O3}	0.3078(9)	0.3105(8)	0.305(1)	0.303(2)
z_{O3}	0.545(1)	0.547(1)	0.546(1)	0.5406(7)
d_1 = Ir-O_1	2 × 2.01(2)	2 × 2.102(7)	2 × 2.04(2)	2 × 1.96(1)
d_2 = Ir-O_2	2 × 2.012(8)	2 × 2.004(6)	2 × 2.048(8)	2 × 2.06(1)
d_3 = Ir-O_3	2 × 2.013(10)	2 × 2.008(7)	2 × 2.032(9)	2 × 2.020(9)
d_0	2.0114	2.0380	2.0383	2.0123
$10^4\,\Delta$	0.012	10.03	0.23	9.31
O-Ir-O (°)	180.0(6)	180.0(11)	180.0(9)	180.0(9)
BVS (IR)	4.09(7)	3.84(3)	3.81(5)	4.11(4)
BVS (Pr)	3.01(4)	3.08(3)	2.89(3)	2.95(3)
BVS (Ni)	1.98(3)	2.15(2)	2.14(3)	1.99(2)
BVS (O_1)	2.03(5)	2.02(2)	1.99(3)	2.12(2)
BVS (O_2)	2.02(3)	2.07(2)	1.94(3)	1.97(3)
BVS (O_3)	1.99(4)	1.97(2)	1.92(3)	1.91(3)
R_{Bragg}	2.9	3.4	2.6	3.2

II. EXPERIMENTAL DETAILS

Polycrystalline samples of Pr_2NiIrO_6 and Nd_2NiIrO_6 have been prepared via solid state reaction [31]. Starting materials of R_2O_3, NiO, and IrO_2 were mixed and ground in stoichiometric ratios. The powder samples were calcined at 900 °C for 24 h and 1100 °C for 48 h, pressed into 10 mm pellets, and annealed at 1200 °C for 24 h. After annealing, the pellets were powdered, and the phase purity was checked at room temperature (RT) using a Rigaku x-ray diffractometer equipped with a Cu-Kα source. DC and AC magnetization as a function of temperature and magnetic field were measured using a superconducting quantum interference device. High-resolution neutron diffraction data were recorded at RT

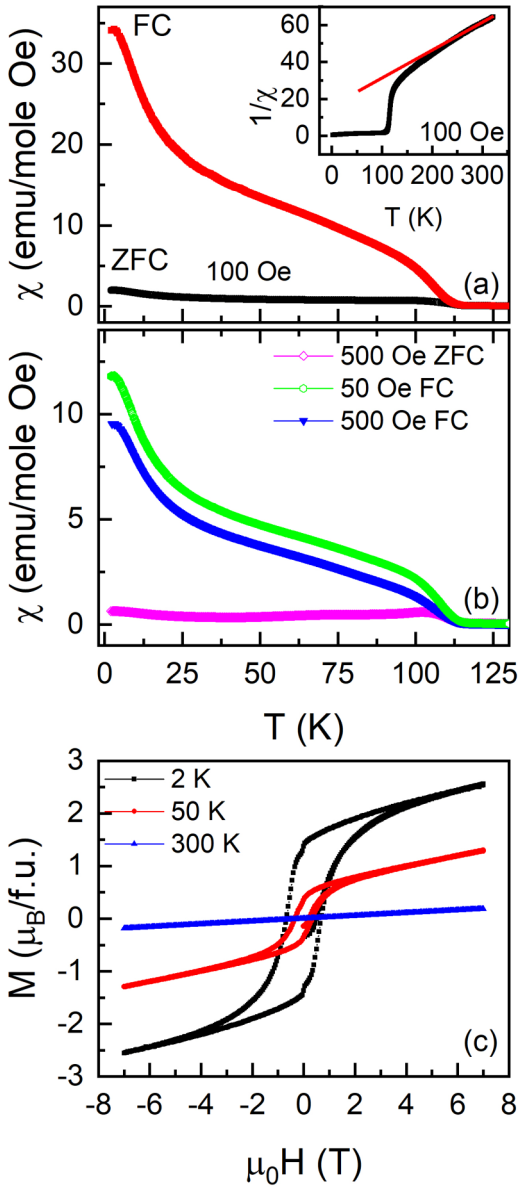

FIG. 2. (a) Temperature dependence of the zero-field-cooled (ZFC) and field-cooled (FC) susceptibility (χ) of Pr_2NiIrO_6 measured with 100 Oe and (b) χ measured with different applied fields. (c) Magnetization isotherms of Pr_2NiIrO_6 measured at different temperatures. A clear hysteresis is visible in the 2 and 50 K data. The inset shows the inverse susceptibility vs temperature curve, and the solid line shows the fit to Curie-Weiss behavior.

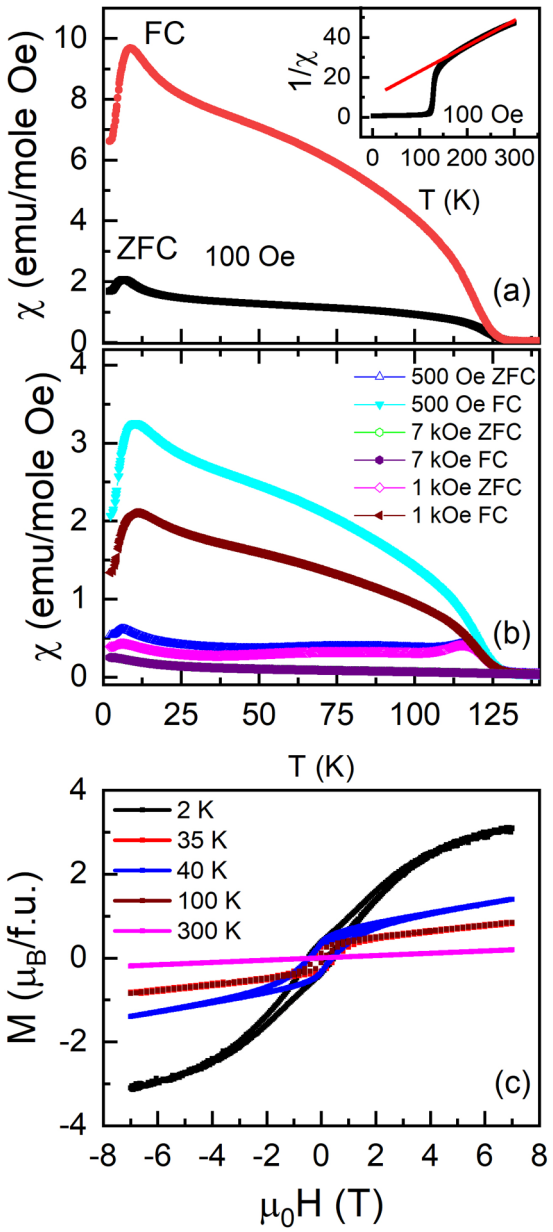

FIG. 3. (a) Temperature dependence of the zero-field-cooled (ZFC) and field-cooled (FC) susceptibility (χ) of Nd_2NiIrO_6 measured with 100 Oe and (b) χ measured with different applied fields. (c) Magnetization isotherms of Nd_2NiIrO_6 measured at different temperatures. A hysteresis is visible in all except the room temperature data. The inset shows the inverse susceptibility vs temperature curve, and the solid line shows the fit to Curie-Weiss behavior.

and 1.5 K on the powder diffractometer D2B at the Institut Laue-Langevin (ILL), Grenoble, France, using a wavelength of $\lambda = 1.594$ Å. The high-intensity neutron powder diffractometer D20, as well at the ILL, was used with $\lambda = 2.415$ Å to record temperature-dependent data between 1.5 and 130 K for Pr_2NiIrO_6 using a ramp speed of 0.1 K every 48 s. Data were recorded for 15 min, giving a temperature resolution of ∼1.88 K. Very long data acquisitions of 2 h each were furthermore taken at $T = 1.5$, 20, 50, 60 and 130 K. Temperature-dependent data of 5 min per spectrum were measured on Nd_2NiIrO_6 between 1.5 and 30 K with a ramp speed of 0.1 K every 15 s, resulting in a spectrum every 2 K. A second temperature ramp (0.1 K every 35 K) spanned the region between 30 and 125 K with data taken for 30 min, resulting in a spectrum every 5 K. Data points with very high statistics were recorded at 1.5 K (2 h) and at 30, 100, and 140 K (4 h each). Rietveld refinements of the powder x-ray diffraction (XRD) and NPD data were performed using FULLPROF [32]. The magnetic form factor of Ir^{4+} as published by Kobayashi *et al.* [33] was used. Symmetry analysis was done using BASIREPS [34,35] and the program MAXMAGN of the Bilbao Crystallographic Server [36].

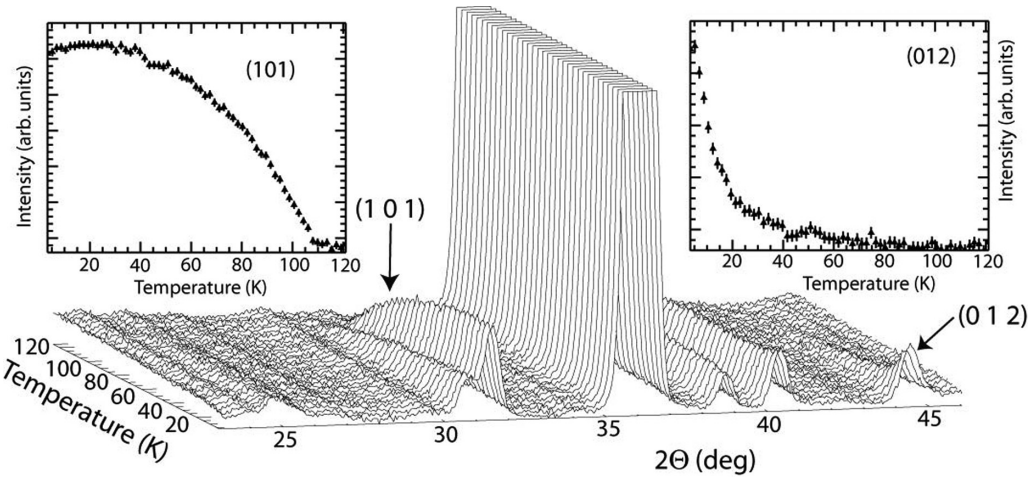

FIG. 4. Thermodiffractogram of Pr_2NiIrO_6 between 1.5 and 120 K showing the appearance of magnetic peaks. The insets show the temperature dependence of the (101) reflection (left) and the (012) reflection (right).

III. RESULTS AND DISCUSSION

A. Crystal structure determination

The Rietveld refinements of the RT XRD data validate the monoclinic symmetry $P2_1/n$ and the absence of any significant impurity phase for both compounds. The cation site disorder between Ni on the Wyckoff site $2b$ $(0, 0, \frac{1}{2})$ and Ir on the site $2a$ $(0, 0, 0)$ can be determined to $< 7\%$ for $R =$ Pr and $< 4\%$ for $R =$ Nd. A slight contamination by a 1% impurity phase of Pt in the Nd compound can be seen in the NPD data and was refined as a secondary phase; Fig. 1 shows the corresponding refinement.

High-resolution NPD data taken at 1.5 K confirm the absence of a structural transition compared with RT for both compounds. The lattice parameters decrease as expected in a and c directions for both compounds, while the unit cell expands slightly in the direction of the b axis. Table I lists the refined values of the lattice constants, atom coordinates, and the resulting Ir-O distances and bond valence sums (BVSs) for both temperatures. The BVSs confirm the supposed valences of R^{3+}, Ni^{2+}, and Ir^{4+}. The distortion of the IrO_6 octahedra Δ, which is nearly absent at RT, increases strongly at 1.5 K in both compounds.

B. Magnetic properties

Figure 2(a) shows the temperature-dependent zero-field-cooled (ZFC) and field-cooled (FC) DC magnetic susceptibility curves of Pr_2NiIrO_6 measured at 100 Oe, while Fig. 2(b) shows the ZFC curve measured after cooling in zero field and then applying 500 Oe and collecting the data from 2 to 130 K. The FC curves were measured with 50 and 500 Oe after cooling the same in applied field. Figure 2(c) displays the magnetization isotherms at three different temperatures. At ∼110 K, a clear transition becomes visible in the susceptibility data which corresponds to the onset of magnetic order, as will be confirmed later from the NPD data. The anomaly visible at this temperature is strongly dependent on the measuring conditions. Changes in the susceptibility behavior with different applied measuring fields are visible in Figs. 2(a) and 2(b). A strong increase can be seen in the FC curve measured with $H = 100$ Oe, while a measuring field of $H = 500$ Oe leads to a small reduction of the anomaly in the FC curve. Magnetic hysteresis indicating a strong ferromagnetic component is visible in the magnetization data at 50 K and even stronger at 2 K [Fig. 2(c)]. A second anomaly is visible in the susceptibility [Figs. 2(a) and 2(b)] at ∼25 K, which should be due to a change in the relative strengths of the magnetic interactions or to the appearance of an additional interaction within the three sublattices. The surprising field dependence of the ZFC and FC susceptibility data points to a delicate balance within a ferrimagnetic order of the three sublattices.

The susceptibility data of Nd_2NiIrO_6 are shown in Figs. 3(a)–3(b). The ZFC data measured with $H = 100$ Oe show two anomalies at ∼120 K and <∼ 25 K [Fig. 3(a)]. The curve gets more structured as the measuring field is increased; see, e.g., the curve for 1 kOe in Fig. 3(b). Without the knowledge from the NPD data, only the first anomaly at ∼120 K can be linked directly to the onset of the magnetic order. Figure 3(c) shows the magnetization data, which reveal again a ferromagnetic component through the presence of a hysteresis.

Comparing Figs. 2(c) and 3(c), it can be seen that while the width of the hysteresis (coercivity) increases strongly when going from 50 to 2 K in Pr_2NiIrO_6, it stays constant between 40 and 2 K in Nd_2NiIrO_6. As will be shown later from the NPD data, this can be explained by the presence of a second magnetic transition to an antiferromagnetic order of a large part of the sample volume of Nd_2NiIrO_6. The Curie-Weiss (CW) fit of the inverse susceptibility data [see the insets in Figs. 2(a) and 3(a)] leads to values of the effective paramagnetic moments (μ_{eff}) and of the CW temperatures (Θ_C) of 7.75 μ_B and −66.9 K for Nd_2NiIrO_6 and 6.61 μ_B and −39.6 K for Pr_2NiIrO_6. These values of μ_{eff} and Θ_C are slightly different from those given by Kayser *et al.* [28], which might be because they used a more extended temperature region (up to 400 K) to do the CW fitting. Although the magnetization curves reveal through their hysteresis the presence of a ferromagnetic component, the negative values of the CW

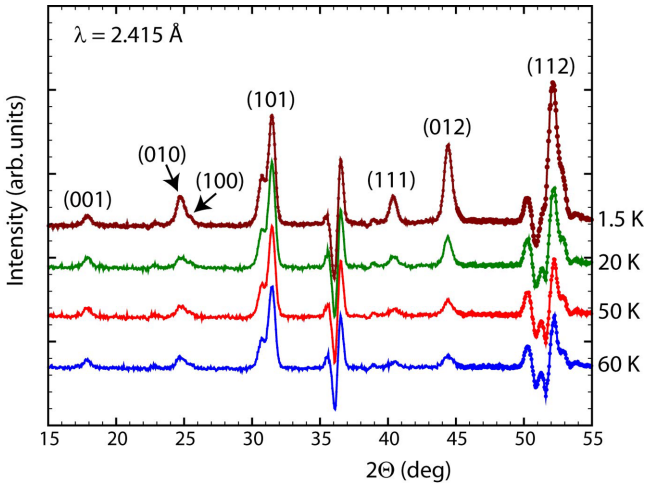

FIG. 5. Intensity of the purely magnetic diffraction at different temperatures as obtained by subtracting the paramagnetic background measured at 130 K. Up-down features as seen, for example, at 36° are created by the thermal shift of strong nuclear reflections.

temperatures point to predominantly antiferromagnetic interactions in both compounds, as confirmed below by neutron diffraction.

C. Magnetic structure determination

1. Pr_2NiIrO_6

The temperature dependence of the high-intensity NPD data of Pr_2NiIrO_6 (Fig. 4) shows the appearance of new Bragg peaks which indicate the onset of magnetic order. The magnetic peaks can be indexed with the magnetic propagation vector $k = 0$ in accordance with Refs. [28,29]. Comparing the temperature dependencies of the magnetic peaks, some clear differences are visible: While, e.g., the (101) reflection (left inset of Fig. 4) appears and increases rapidly < 110 K, the (012) reflection (right inset) shows a strong increase only < 20 K and is hardly visible > 60 K. While the first reflection (101) is used to define $T_C = 110$ K, the second (012) can be linked to the development of the magnetic moment of the rare earth, intrinsic < 20 K and probably induced by the magnetic order of the Ni and Ir sublattices > 20 K, as will be discussed in more detail below.

The different temperature dependencies of the magnetic reflections are best seen when looking at the difference data files (Fig. 5) created by subtracting the paramagnetic background measured at 130 K from the data taken with high statistics at 1.5, 20, 50, and 60 K. Instead of using the pure data, which contain the nuclear and the magnetic scattering, we will use for the refinement of the magnetic structures these difference datasets. This strongly increases the sensibility to the details of the magnetic structure. The better quality of these difference datasets due to the strongly improved statistics compared with those used in Ref. [28] can be noted.

Magnetic symmetry analysis for the three cation sites was done using the program BASIREPS [34,35]. Table II lists the allowed IRs and their basis vectors (BVs). There are two identical IRs for Ni and Ir, each having 3 BVs, while there are 4 IRs each with 3 BVs for Pr. As the magnetic data clearly indicate, the presence of a strong ferromagnetic contribution IR2 and IR4 which contain solely BVs describing an antiferromagnetic interaction can be excluded as possible solutions. IR1 allows a ferromagnetic coupling in direction of the unit cell b direction (BV2), while IR3 allows ferromagnetic couplings in the a and c directions (BV1 and BV3).

Testing these two IRs against the measured data, it becomes immediately clear that only IR1 (corresponding to the magnetic space group $P2_1/c$, see as well Ref. [29]) can reproduce the magnetic diffraction intensities. The refinement using IR1 allows us in principle to use nine free variables to describe the magnetic structure of the three magnetic cations. This can lead to unstable fits at higher temperatures where the magnetic diffraction intensities are not yet strong.

Figure 6(a) shows the best refinement of the data at 1.5 K; values of the magnetic components of the three cations in the three directions of the BVs are listed in Table III. IR1 corresponds to the IR already employed by Kayser *et al.* [28] and by Ferreira *et al.* [29] for the refinement of their data on Pr_2NiIrO_6. The data used in Ref. [28] were collected on the high-resolution powder diffractometer D2B and suffer from very low statistics of the magnetic peaks within a relatively high background. Figure 6(b) presents a refinement of the difference data file using the results of Ref. [28] which proposed a ferromagnetic component for Ni in the b direction (BV2) with $\mu_b = 2.3\,\mu_B$, strong antiferromagnetic components (BV1, BV3) in the a and c directions ($\mu_a = 1.3\,\mu_B$, $\mu_c = 1.6\,\mu_B$) for Ir, and a further antiferromagnetic contribution in the a direction of $\mu_a = 0.93\,\mu_B$ originating from

TABLE II. BVs of the allowed IRs for $k = 0$ for the Wyckoff positions 4*e*, 2*b*, and 2*a* of the space group $P2_1/n$. IR1 is highlighted, as it corresponds to the IR used to describe the magnetic structure of Pr_2NiIrO_6 and that of Nd_2NiIrO_6 for $T > 15$ K.

	IR1			IR2			IR3			IR4		
R on 4*e*	**BV1**	**BV2**	**BV3**	BV1	BV2	BV3	BV1	BV2	BV3	BV1	BV2	BV3
x, y, z	**1 0 0**	**0 1 0**	**0 0 1**	1 0 0	0 1 0	0 0 1	1 0 0	0 1 0	0 0 1	1 0 0	0 1 0	0 0 1
$-x+\frac{1}{2}, y+\frac{1}{2}, -z+\frac{1}{2}$	**−1 0 0**	**0 1 0**	**0 0 −1**	−1 0 0	0 1 0	0 0 −1	1 0 0	0 −1 0	0 0 1	1 0 0	0 −1 0	0 0 1
$-x, -y, -z$	**1 0 0**	**0 1 0**	**0 0 1**	−1 0 0	0 −1 0	0 0 −1	1 0 0	0 1 0	0 0 1	−1 0 0	0 −1 0	0 0 −1
$x+\frac{1}{2}, -y+\frac{1}{2}, z+\frac{1}{2}$	**−1 0 0**	**0 1 0**	**0 0 −1**	1 0 0	0 −1 0	0 0 1	1 0 0	0 −1 0	0 0 1	−1 0 0	0 1 0	0 0 −1
Ni (2*b*), Ir (2*a*)												
x, y, z	**1 0 0**	**0 1 0**	**0 0 1**				1 0 0	0 1 0	0 0 1			
$-x+\frac{1}{2}, y+\frac{1}{2}, -z+\frac{1}{2}$	**−1 0 0**	**0 1 0**	**0 0 −1**				1 0 0	0 −1 0	0 0 1			

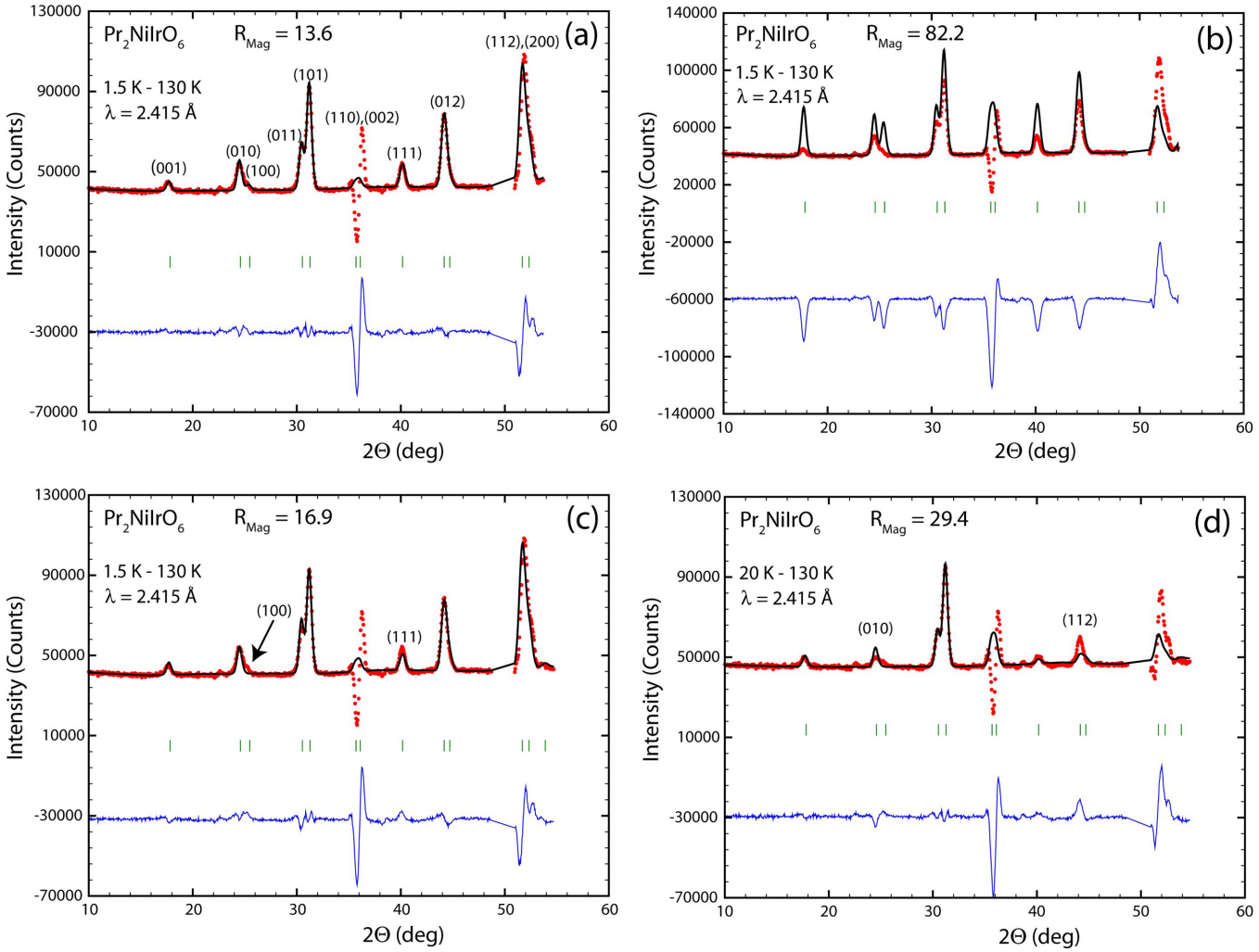

FIG. 6. (a) Refinement of the difference data set 1.5–130 K of Pr_2NiIrO_6. (b) The same, using the results of [28]. (c) The same but excluding the magnetic component in the c direction (BV3). (d) Refinement of the difference dataset 20–130 K excluding any magnetic contribution from Pr.

Pr. One notices strong differences between the calculated and observed curves including a general overestimation of the magnetic diffraction intensities but as well inconsistencies in the relative intensities of the magnetic peaks. Comparing this solution with the magnetic structure model proposed here (Table III), one remarks as main differences the >3 times larger value of the total magnetic moment of Ir (2.1 μ_B compared with 0.59 μ_B) and a ferromagnetic contribution created solely by Ni in the b direction which leads to the largely overestimated magnetic contribution to the (110)/(200) couple of peaks at $2\Theta = 36^\circ$ which have a 20 times stronger nuclear contribution. As the refinement in Ref. [28] used the pure data and not a difference data file, this problem was easily hidden.

Compared with the results presented in Ref. [29], the differences are only subtle and are at 1.5 K mostly limited to the additional components in the c direction (BV3) found here but excluded in Ref. [29]. Ignoring this component, the magnetic R factor increases from 13.6 to 16.9. Figure 6(c) shows visually the effect of excluding this additional component allowed in IR1: While the magnetic (111) reflection is only missing some calculated intensity, the magnetic (100) reflection (see arrow) is not calculated at all. In this context, we would like to mention that both misfits are slightly discernable even in the original refinement as shown in Fig. 3(e) of Ref. [29]. Differently to Ref. [28] but in accordance with our results, a ferrimagnetic alignment along the b direction between Ni/Pr and Ir was proposed in Ref. [29]. The total magnetic moment values found in Ref. [29] were $\mu_{Ni} = 1.63(4)\,\mu_B$, $\mu_{Ir} = 0.39(7)\,\mu_B$, and $\mu_{Pr} = 1.58(3)\,\mu_B$, similar to those found here [$\mu_{Ni} = 1.79(6)\,\mu_B$, $\mu_{Ir} = 0.59(8)\,\mu_B$, and $\mu_{Pr} = 1.21(4)\,\mu_B$, Table III]. The additional component along the c direction (BV3) is still present at higher temperatures, as indicated by the persistence of the (100) reflection (Fig. 5). Due to its reduced intensity and due to the overall decrease in the magnetic diffraction intensity, this component was, however, excluded from the refinements of the difference datasets at 20, 50, and 60 K, limiting the number of magnetic parameters to six and leading to more stable fits. Table III includes the results of the refinements at these higher temperatures. Contrary to Ref. [29], we must include a magnetic contribution from Pr in the refinement of the difference dataset at 20, 50, and 60 K data. To illustrate this, we have plotted in Fig. 6(d) the best

TABLE III. Total magnetic moments and their components in the direction of the unit cell axes at different temperatures of Pr_2NiIrO_6 resulting from the refinement of difference data files. The component in the c direction (BV3, Table II) was only refined at 1.5 K. For details see the main text.

	60 K	50 K	20 K	1.5 K
		Ni		
μ_a	0.64(3)	0.69(3)	0.81(3)	0.70(4)
μ_b	1.40(4)	1.47(4)	1.65(5)	1.54(5)
μ_c	–	–	–	−0.57(5)
μ_{Ni}	1.54(5)	1.62(4)	1.84(5)	1.79(6)
		Ir		
μ_a	0.23(3)	0.24(3)	0.32(3)	0.20(5)
μ_b	−0.34(4)	−0.36(5)	−0.32(5)	−0.50(5)
μ_c	–	–	–	−0.23(5)
μ_{Ir}	0.41(4)	0.43(4)	0.45(5)	0.59(8)
		Pr		
μ_a	0.07(2)	0.09(2)	0.21(2)	0.77(3)
μ_b	0.13(3)	0.16(3)	0.35(4)	0.92(4)
μ_c	–	–	–	0.12(3)
μ_{Pr}	0.14(4)	0.18(4)	0.41(4)	1.21(4)
R_{Mag}	27.7	26.6	20.9	13.6

refinement of the 20 K data excluding any magnetic moment on the Pr site ($R_{Mag} = 29.4$ compared with 20.9 when including a Pr moment, see Table III). Misfits of the (010) and (112) reflections are clearly visible. Furthermore, strong intensity is created on the (110)/(200) couple of peaks at $2\Theta = 36°$, a region which had been excluded from the refinement in Ref. [29]. One must comment here that the relatively high values of R_{Mag} (Table III) are mostly due to the presence of the up-down features at, e.g., $2\Theta = 36°$ and 52 ° created by the thermal shift of the nuclear peaks. As already mentioned above, when discussing the results of Ref. [28] and as seen when refining the 20 K data without contribution from Pr [Fig. 6(d)], it is imperative to include these regions in the refinements, as the information on a possible magnetic contribution to the Bragg peaks at these positions is crucial for the refinements. Fixing all parameters to the obtained values but excluding the regions around $2\Theta = 36°$ and 52°, the magnetic R factors decrease, e.g., to $R_{Mag} = 5.4$ for both the 1.5 and 60 K refinements, confirming the inherent quality of the fits.

Figure 7(a) displays the evolution of the total magnetic moments of the three sites: while Ni and Ir have already achieved the largest part of their low-temperature magnetic moment values at 60 K, the Pr moment—although already present at 60 K—sees a strong increase only < 20 K. This confirms the interpretation in terms of intrinsic and induced Pr moments as put forward above when discussing the different temperature dependencies of the (101) and (012) reflections (insets of Fig. 4). A picture of the magnetic structure of Pr_2NiIrO_6 at 1.5 K is shown in Fig. 7(b).

In Ref. [29], it has been proposed that, in Pr_2NiIrO_6, the Ni moment should be regarded as the dominant one, while the Ir moment should be seen as being induced. As we have no data close to the magnetic transition temperature (at 60 K, both sublattices are already well ordered), we cannot confirm or refute this interpretation, but we can point out here that, in La_2ZnIrO_6 [27], where Ir represents the only magnetic ion, the Ir magnetic order appears intrinsically. La_2ZnIrO_6 possesses the same nuclear structure and the same magnetic propagation vector $k = 0$. The magnetic order developed in La_2ZnIrO_6 by the Ir sublattice follows, however, not IR1 as in Pr_2NiIrO_6 but IR3 (see Table II) and appears only at 7.5 K. Both facts could therefore speak in favor of an induced character of the magnetic order of the Ir sublattice in Pr_2NiIrO_6 in the high-temperature range below $T_C = 110$ K.

2. Nd_2NiIrO_6

Figure 8(a) displays the thermal dependence of the high-intensity NPD data of Nd_2NiIrO_6 between 1.5 and 120 K. A first transition leads to the appearance of magnetic peaks at ∼120 K, while a second transition starts at ∼15 K. Indexing the new magnetic peaks, it becomes clear that the first transition corresponds to the development of a magnetic

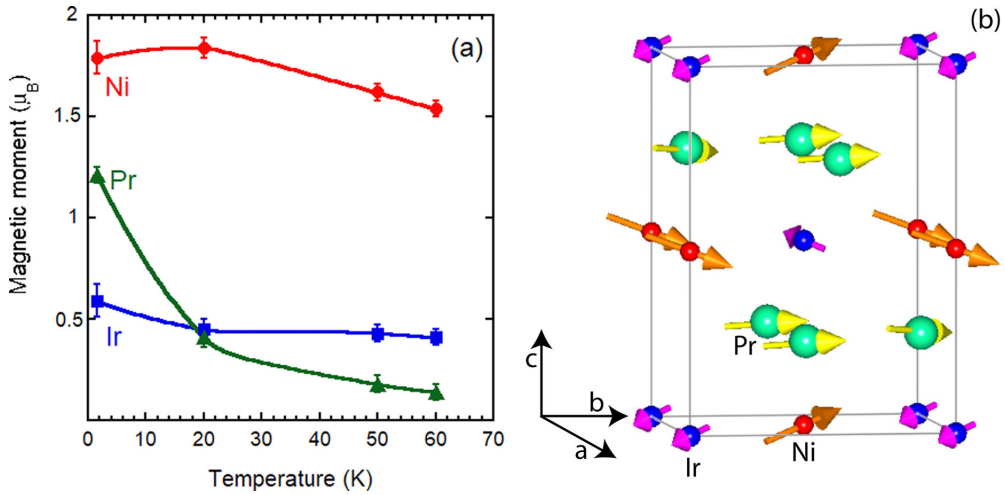

FIG. 7. (a) Temperature dependence of the total magnetic moments of the three cation sites of Pr_2NiIrO_6. (b) Magnetic structure of Pr_2NiIrO_6 at 1.5 K. A ferrimagnetic alignment along the b direction between Ni/Pr on one hand and Ir on the other hand represents the main component of the magnetic structure.

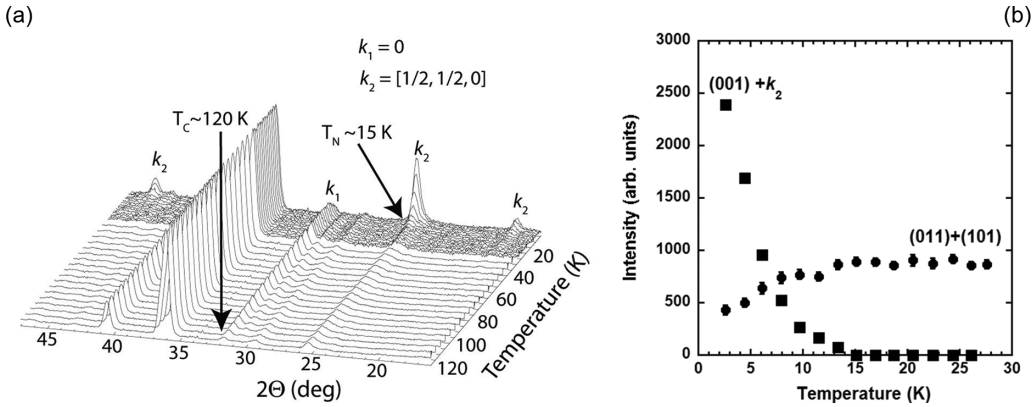

FIG. 8. (a) Thermodiffractogram of Nd_2NiIrO_6 between 1.5 and 120 K showing the appearance of magnetic peaks $<\sim 120$ K and <15 K. (b) The variation with temperature of the intensity of magnetic peaks characteristic for the two magnetic phases in the temperature range of T_N.

structure with $k_1 = 0$, as already found for Pr_2NiIrO_6. However, contrary to the situation found in Pr_2NiIrO_6, the second transition at 15 K is not corresponding to a change within the existing magnetic order but to the appearance of a new magnetic structure with $k_2 = (\frac{1}{2}, \frac{1}{2}, 0)$. Concomitant with the emergence of the new order, the magnetic peaks, created by the old order with $k_1 = 0$, decrease in intensity without, however, disappearing completely. At 1.5 K, a coexistence of both types of magnetic order persists, as can be seen in Fig. 8(b), which shows the intensity of two characteristic magnetic Bragg peaks. While the $(001) + k_2$ peak appears rapidly <15 K, the intensity of the coupled (011) + (101) peaks, which are created by the $k_1 = 0$ order, decreases by $\sim> 50\%$ between 15 K and the base temperature.

The refinement of the magnetic structures uses again difference data files created by subtracting high statistic data taken in the paramagnetic state at 140 K from long measurement at 1.5, 30, and 100 K. There exist two different possibilities to refine the data within the range of $120\,\text{K} > T > 15\,\text{K}$: Both recall the $k = 0$ type magnetic order found for Pr_2NiIrO_6 and use the same IR1 (Table II). Assuming magnetic order only on the Ni and Ir sites, the first solution ($R_{\text{Mag}} = 9.7$) sees a large magnetic moment on the Ir site pointing in the direction of the b axis ferrimagnetically aligned to the μ_b component of the Ni site. Moment values at 30 K are in this model: $\mu_{\text{Ir}} = 1.02\,\mu_B$ [$\mu_a = 0.23(2)\,\mu_B$, $\mu_b = -0.99(22)\,\mu_B$, and $\mu_c = 0.00(7)\,\mu_B$] and $\mu_{\text{Ni}} = 1.21\,\mu_B$ [$\mu_a = 0.67(2)\,\mu_B$, $\mu_b = 0.95(20)\,\mu_B$, and $\mu_c = 0.32(6)\,\mu_B$]. This model corresponds in some respect to the solution proposed by Ferreira *et al.* [29] for the magnetic structure of Nd_2NiIrO_6 at 40 K. In Ref. [29], however, only magnetic components of $\mu_{\text{Ni}} = 1.71(2)\,\mu_B$ and $\mu_{\text{Ir}} = 0.32(7)\,\mu_B$ ferrimagnetically aligned along the b axis were found. Figure 9(b) displays a refinement ($R_{\text{Mag}} = 72$) of our difference data at 30 K using their model: The majority of the magnetic peaks is not refined, and strong intensity is created at the position of the (110)/(002) peaks at $2\Theta \sim 36^\circ$. The absence of calculated intensity on most of the magnetic peaks results from absence of the antiferromagnetic components of IR1 represented by BV1 and BV3 (Table II). These components were neglected in Ref. [29], as the created magnetic peaks were not visible in their difference data due to low statistics and high background. The misfit at $2\Theta \sim 36^\circ$ results from the large difference between the magnetic moment values of Ni and Ir ferrimagnetically aligned in the b direction and was hidden in Ref. [29] by the large background. Similar but anti-aligned values of the BV2 components of Ni and Ir lead to the absence of intensity on the (110)/(002) peaks and correspond to our first solution. The relatively large value of Ir ($1.02\,\mu_B$) found in this solution is, however, surprising in comparison with the results of Pr_2NiIrO_6 (see Sec. III C 1) and La_2NiIrO_6 [29,30] where values of ~ 0.2–$0.6\,\mu_B$ were determined. For Pr_2NiIrO_6, we had realized that an induced magnetic moment exists on the Pr site already at temperatures significantly higher than $T = 20$ K

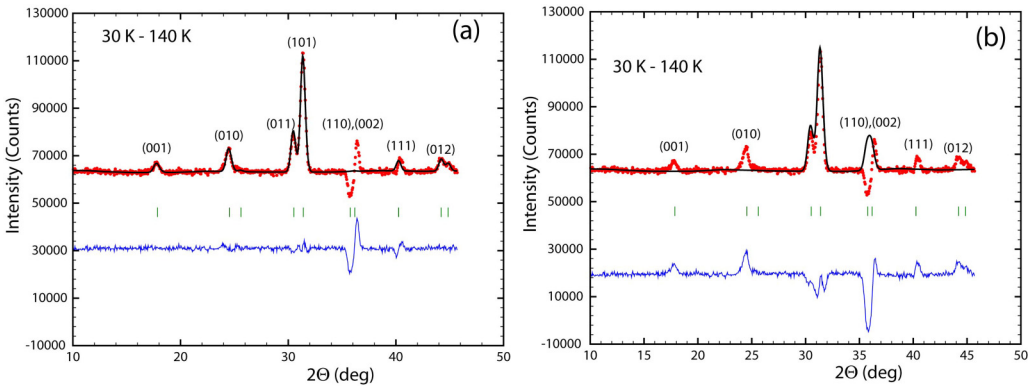

FIG. 9. (a) Refinement of the difference dataset 30–130 K of Nd_2NiIrO_6. (b) The same using the results of [29].

TABLE IV. Total magnetic moments and their components of Nd_2NiIrO_6 in the $k_1 = 0$ phase at 100 and 30 K.

	100 K	30 K
	Ni	
μ_a	0.39(2)	0.65(2)
μ_b	0.83(21)	1.39(17)
μ_c	0.14(9)	0.23(9)
μ_{Ni}	0.93(21)	1.55(18)
	Ir	
μ_a	0.18(2)	0.23(2)
μ_b	−0.40(23)	−0.42(19)
μ_c	–	–
μ_{Ir}	0.44(23)	0.48(20)
	Nd	
μ_a	–	–
μ_b	0.27(13)	0.56(10)
μ_c	–	–
μ_{Nd}	0.27(13)	0.56(10)
R_{Mag}	8.6	8.0

where a strong increase due to intrinsic order of the rare earth site starts (Fig. 4, Table III). In our second solution to refine the difference data of Nd_2NiIrO_6 at 30 K, we allowed correspondingly the presence of a magnetic moment as well on the Nd site. The resulting refinement ($R_{Mag} = 8.0$) is shown in Fig. 9(a). Table IV contains the determined magnetic moment values and their components at 30 and 100 K where the same model was used. The magnetic moment of Ir adopts now values in the expected range; the resulting magnetic structure is like the one found for Pr_2NiIrO_6 [Fig. 7(b)]. As well due to the slightly lower R_{Mag} value, this solution is therefore preferred. It recalls the ferrimagnetic alignment of Ni and Ir along the *b* axis described in Ref. [29] adds, however, relative to Ref. [29] a ferromagnetic contribution of the Nd site and antiferromagnetic components described by BV1 and BV3. Kayser *et al.* [28] refined the magnetic structure of Nd_2NiIrO_6 only at $T = 5$ K. They assumed, at this temperature, a magnetic structure having only $k = 0$, which is contradicting our results and those of Ref. [29], where the presence of a $k = (\frac{1}{2}, \frac{1}{2}, 0)$ type magnetic structure was found at low temperatures.

To refine the magnetic structure at 1.5 K, we used the program MAXMAGN of the Bilbao Crystallographic server [36] to perform symmetry analysis of the three cation sites with $k = (\frac{1}{2}, \frac{1}{2}, 0)$ in $P2_1/n$. Only one solution corresponding to the magnetic space group 2-P_s-1 (No. 2.7) allows the presence of magnetic moments on all three sites. Under the action of the magnetic propagation vector, the sites get split, creating two independent Nd, Ni, and Ir sites. Each of these independent cation sites possesses three BVs, and a refinement can in theory use 18 independent parameters to describe the magnetic structure. As already successfully done in the case of La_2NiIrO_6 [30], we restricted the components of the split sites to adopt the same absolute values, reducing the number of variables to nine and stabilizing thereby the refinement. In Ref. [30], we explained for the case of La_2NiIrO_6 that different relative orientations of the components of the Ni and Ir magnetic moments can produce equivalently good refinements. This ambiguity relates to the fact that both Ni and Ir are occupying in $P2_1/n$ special positions having site inversion symmetry. The situation is different in Nd_2NiIrO_6, as now the magnetic diffraction from the rare earth on the general position 4*e* adds information on the relative orientation of the different contributions, leading to different R_{Mag} values between the models. Due to the persistence of the $k_1 = 0$ type magnetic structure at low temperatures, a two-phase refinement of the difference dataset 1.5–140 K was done by partitioning the nuclear scale factor between the two magnetic phases. The magnetic moment values of the $k_1 = 0$ phase were fixed here to the values determined from the 30 K data (Table IV), as it is not possible to refine the magnetic moment values and the partial scale factor at the same time. This is obviously an approximation, as at least the rare earth moment should increase when going to lowest temperatures, as seen for the case of Pr_2NiIrO_6 (Table III). On the other hand, the refinement of the difference dataset 1.5–140 K shows that the magnetic scattering of the $k_1 = 0$ phase represents only ∼8% of the total magnetic scattering intensity, so that a small error in the assumed magnetic moment values should not very strongly affect the results for the $k_2 = (\frac{1}{2}, \frac{1}{2}, 0)$ phase. Table V lists the magnetic components of the three cation sites corresponding to the best refinement of the $k_2 = (\frac{1}{2}, \frac{1}{2}, 0)$ phase using only five variables for the description of the magnetic structure ($R_{Mag} = 4.2$); Fig. 10 shows the plot of the resulting refinement. It must be mentioned that, due to the possible underestimation of the fixed magnetic moments of the $k_1 = 0$ phase, the values given in Table V for the $k_2 = (\frac{1}{2}, \frac{1}{2}, 0)$ phase might by overestimated by 10–15%. Instead of assuming the coexistence of two magnetic phases having different magnetic propagation vectors in different parts of the sample volume, as done here, one could as well explain the different magnetic reflections at low temperatures as resulting from a magnetic order possessing both *k* vectors simultaneously throughout the whole sample. This possibility cannot be excluded but seems very unlikely as the superposition of the $k_1 = 0$ order with the $k_2 = (\frac{1}{2}, \frac{1}{2}, 0)$ order would lead to a

TABLE V. Values of the total magnetic moments and their components in the $k_2 = (\frac{1}{2}, \frac{1}{2}, 0)$ type phase in Nd_2NiIrO_6 at 1.5 K.

	(100)	(010)	(001)	μ (μ_B)
Nd1 on 4*e* (*x*, *y*, *z*)	–	−1.98(2)	0.32(5)	2.01(2)
Nd2 on 4*e* $(-x+\frac{1}{2}, y+\frac{1}{2}, -z+\frac{1}{2})$	–	1.98(2)	0.32(5)	2.01(2)
Ni1 on 0 0 $\frac{1}{2}$	−1.84(8)	–	−0.72(6)	1.98(6)
Ni2 on $\frac{1}{2}$ $\frac{1}{2}$ 0	1.84(8)	–	−0.72(6)	1.98(6)
Ir1 on 0 0 0	–	−0.37(5))	–	0.37(5)
Ir2 on $\frac{1}{2}$ $\frac{1}{2}$ $\frac{1}{2}$	–	0.37(5))	–	0.37(5)

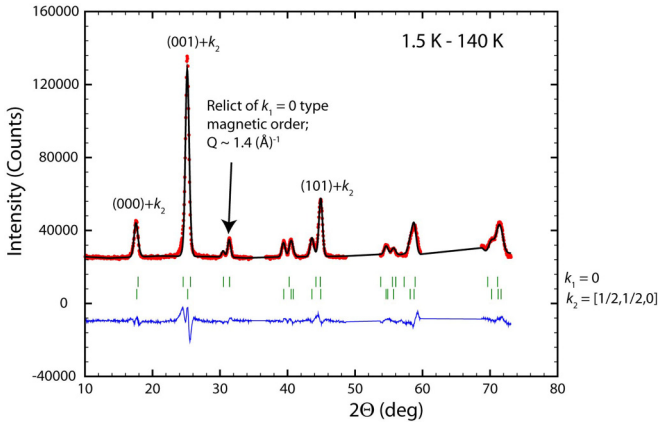

FIG. 10. Refinement of the difference dataset 1.5–130 K of Nd_2NiIrO_6 using a two-phase model where part of the sample volume keeps the high temperature $k_1 = 0$ type magnetic structure, while the other part adopts the $k_2 = (\frac{1}{2}, \frac{1}{2}, 0)$ type order. Observed (dots, red), calculated (line, black), and difference pattern (line, blue). The tick marks indicate the calculated position of the Bragg reflections of the $k_1 = 0$ phase (upper row) and $k_2 = (\frac{1}{2}, \frac{1}{2}, 0)$ phase (lower row).

very complicated magnetic structure having strongly differing magnetic moment values within the same sublattices. The fact that the structurally similar La_2NiIrO_6 [30] adopts at low temperatures the $k_2 = (\frac{1}{2}, \frac{1}{2}, 0)$ type magnetic order while Pr_2NiIrO_6 (see Sec. III C 1) adopts the $k_1 = 0$ type magnetic order suggests that both magnetic orders are energetically close in the R_2NiIrO_6 compounds discussed here, explaining thereby possibly the separation into two magnetically differently ordered parts of the sample volume, as postulated for Nd_2NiIrO_6 <15 K.

Figure 11 gives two different views of the magnetic structure of the $k_2 = (\frac{1}{2}, \frac{1}{2}, 0)$ phase of Nd_2NiIrO_6 at 1.5 K. It can be compared with the one found for La_2NiIrO_6 [30] which is as well characterized by $k = (\frac{1}{2}, \frac{1}{2}, 0)$. The structures are very similar, as the magnetic moment of the Ni site is in La_2NiIrO_6 as well oriented mainly in the direction of the a axis, while that of the Ir site points as well mainly along the b axis. The relative orientation of the components of the Ni1 and Ni2 sites and of the two Ir sites (Table V) correspond to one of the three possible solutions proposed for La_2NiIrO_6. It is therefore tempting to propose that this solution (Fig. 8(b) of Ref. [30]) should be—in accordance with the situation in Nd_2NiIrO_6—the most probable one for La_2NiIrO_6.

Comparing Figs. 11(a) and 11(b) with the magnetic structure proposed by Ferreira *et al.* (see Fig. 2(g) of Ref. [29]), two main differences can be pointed out. While in Ref. [29] all three cation sites possess components along the unit cell b direction but not in any other direction, our model sees the main component of the Ni site pointing in the a direction with additional components along the c direction for Ni and Nd. The magnetic moment values [$\mu_{Nd} = 2.20(4)\,\mu_B$, $\mu_{Ni} = 1.27(4)\,\mu_B$, and $\mu_{Ir} = 0.32(5)\,\mu_B$] given in Ref. [29] are not very different from those determined here (Table V). A further difference to the results of Ref. [29] consists in the partial persistence of the $k_1 = 0$ phase at low temperatures found here. This was overlooked in Ref. [29] due to the low magnetic scattering power of this phase and the high overall background. A close look reveals, though, some slight indication of this phase in their data (see Fig. 2(e) of Ref. [29]) at $Q \sim 1.4\,\text{Å}^{-1}$. Neither the magnetic propagation vector of the main magnetic low-temperature phase nor the magnetic moment values given in Ref. [28] are compatible with our data. As already mentioned above, when discussing Pr_2NiIrO_6, the very weak magnetic scattering intensity of the high-resolution data used in Ref. [28] do not allow a detailed analysis of a magnetic phase containing three magnetic cation sites. The closeness of some of the reflections created by $k_1 = 0$ and by $k_2 = (\frac{1}{2}, \frac{1}{2}, 0)$ can be seen in Fig. 10 and explains the misinterpretation of the magnetic propagation vector of Nd_2NiIrO_6 at low temperatures in Ref. [28].

Comparing the magnetic structure of Nd_2NiIrO_6 at low temperature with the one reported for Nd_2ZnIrO_6 [27], both follow the $k = (\frac{1}{2}, \frac{1}{2}, 0)$ propagation vector, and both adopt the magnetic space group 2-P_s-1 (No. 2.7). The coupling

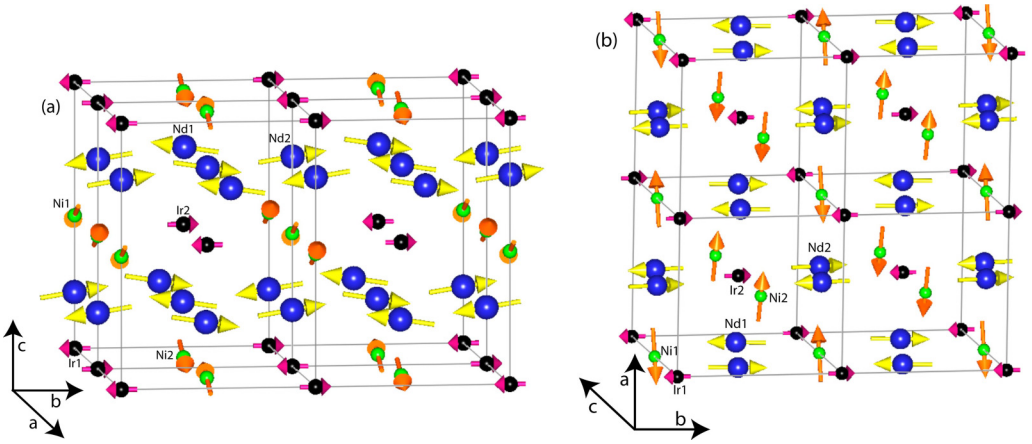

FIG. 11. (a) View of the magnetic structure of the $k_2 = (\frac{1}{2}, \frac{1}{2}, 0)$ phase of Nd_2NiIrO_6 at 1.5 K projected along the a direction. (b) The same projected along c. Indicated are the magnetic Ir (black), Ni (green), and Nd (blue) atoms. The size of the magnetic moment of Ir was rescaled to facilitate its visibility.

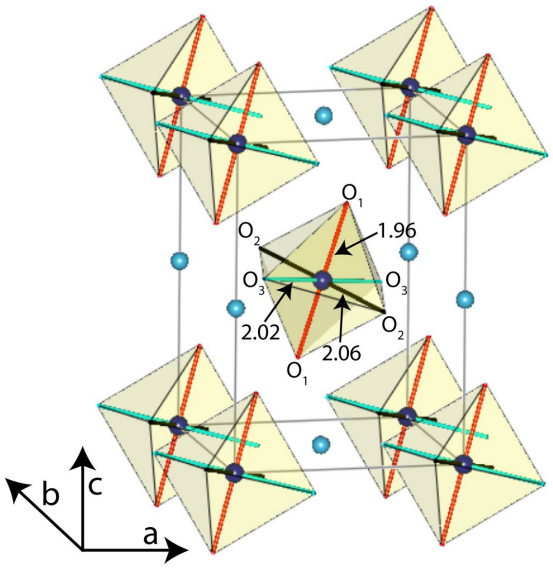

FIG. 12. Octahedral coordination of Ir (black balls) by oxygen. Ni (blue balls), R not shown. Bond lengths given correspond to Nd_2NiIrO_6 at 1.5 K.

between the two independent Nd sites and between the two independent Ir sites (see Table IV for Nd_2NiIrO_6) is, however, different as, e.g., the coupling between the (010) components of Nd1 and Nd2 is parallel in Nd_2ZnIrO_6. The same difference is valid for the (010) components of Ir1 and Ir2, which are parallel in Nd_2ZnIrO_6 but antiparallel in Nd_2NiIrO_6.

D. Magnetic moment values

Magnetic moment values of about $\mu_{Ir} = 0.59\,\mu_B$ and $\mu_{Ir} = 0.37\,\mu_B$ found at 1.5 K for Pr_2NiIrO_6 and Nd_2NiIrO_6 are in line with those found for iridium in La_2NiIrO_6 of $\mu_{Ir} = 0.35\,\mu_B$ [30] but smaller than $\mu_{Ir} \sim 0.7\,\mu_B$ and $0.9\,\mu_B$ found for the double perovskites Nd_2ZnIrO_6 and La_2ZnIrO_6 [27], respectively. In the classical $J = \frac{1}{2}$ model, the spin and orbital moments of Ir^{4+} are taken as having opposite directions, while in the $J_{eff} = \frac{1}{2}$ model, they are considered parallel [19]. While the first model leads to an expected magnetic moment of $\frac{1}{3}$ μ_B, the single electron in the $J_{eff} = \frac{1}{2}$ orbital should lead in the second model to a magnetic moment of $1\,\mu_B$. The values determined here for Pr_2NiIrO_6 ($0.59\,\mu_B$) and Nd_2NiIrO_6 ($0.37\,\mu_B$) seem to contradict the $J_{eff} = \frac{1}{2}$ model due to their small size. There are, however, two reasons which can explain a reduction of the magnetic moment within the $J_{eff} = \frac{1}{2}$ model: Any hybridization between the Ir $5d$ orbitals with the $2p$ orbitals of the coordinating oxygens should lead to a reduction of the moment value [37]. The magnetic moment can be reduced as well if the perfect octahedral surrounding which is the basis of the pure $J_{eff} = \frac{1}{2}$ state is distorted [38]. As shown by Brown and Shannon [39], the covalency of a bond can be related to the bond strength which itself is related to the bond length. Looking at the BVSs of the two compounds at 1.5 K (Table I), there are no apparent deviations from the expected valences of Ir^{4+}, R^{3+}, Ni^{2+}, and O^{2-}. Slightly increased BVS values of 4.12 for Ir and 2.12 for O1 and the reduced bond length Ir-O1 of 1.96 Å at 1.5 K (Fig. 12) could, however, speak in favor of a stronger hybridization between these atoms and a stronger covalency in the Nd compound and explain partly the strong reduction of the Ir moment to $\mu_{Ir} = 0.37\,\mu_B$. Pr_2NiIrO_6 having $\mu_{Ir} = 0.59\,\mu_B$ at 1.5 K does not show any such increased BVS. Table I shows, however, that the nearly perfect cubic octahedral surrounding of Ir present in both compounds at RT gets strongly distorted at 1.5 K. The distortion is of tetragonal type in Pr_2NiIrO_6 with a strongly enlarged apical Ir-O1 distance, while an orthorhombic distortion with three different Ir-O bond lengths (Fig. 12) is present in Nd_2NiIrO_6.

The Nd [$\mu_{Nd} = 2.01(2)\,\mu_B$] and Pr [$\mu_{Pr} = 1.21(4)\,\mu_B$] moments found at 1.5 K are lower than the free-ion values of $3.27\,\mu_B$ expected for Nd^{3+} and $3.2\,\mu_B$ for Pr^{3+}. Similar reduced Nd moments have been found in Nd_2ZnIrO_6 [27] and $Nd_2Na\mathit{B}O_6$ (B = Ru, Os) [40] and were linked to crystal electric field effects. Looking at Figs. 4 (right inset) and 8(b), it appears that, even at the lowest measurement temperature of 1.5 K, the magnetic Bragg peaks reflecting mostly the contribution of the rare earth magnetic moment are still strongly increasing with decreasing temperatures, suggesting that they have not reached their final saturated values at 1.5 K.

IV. CONCLUSIONS

The magnetic structures of the double perovskites Pr_2NiIrO_6 and Nd_2NiIrO_6 have been redetermined using high-intensity neutron diffraction data. Comparing different refinements, the need for high-quality data and the use of difference data files not excluding certain angular regions are shown to explain the difficulties in determining the correct magnetic structures met in previous reports on these compounds. In Pr_2NiIrO_6, a $k = 0$ order sets in below $T_C = 110$ K and consists mainly of a ferrimagnetic alignment of magnetic moments along the monoclinic b axis. The moment directions of the Ni and the Pr sublattices are parallel, while the one of Ir is anti-aligned. Additional antiferromagnetic interactions exist along the a and c directions, leading to total moments of ~1.8, 0.6, and $1.2\,\mu_B$ for Ni, Ir, and Pr, respectively, at 1.5 K. Strongly increasing < 20 K, an induced moment is already present on the Pr site at least up to 60 K. These results are strongly differing from those presented earlier by Kayser *et al.* [28] but confirm partly those presented by Ferreira *et al.* [29], while adding several details. Nd_2NiIrO_6 sees below $T_C = 120$ K a magnetic structure very similar to Pr_2NiIrO_6 with $k = 0$ and a ferrimagnetic alignment along the b axis between Ni/Nd and Ir moments. An induced magnetic moment on the Nd site is confirmed to be present still close to T_C at 100 K. The presence of this Nd moment at high temperatures and additional small antiferromagnetic components in the a and c directions had not been detected in Ref. [29]. Below $T_N = 15$ K, a second type of magnetic order with $k = (\frac{1}{2}, \frac{1}{2}\ 0)$ replaces progressively the high temperature $k = 0$ type structure which, however, survives partly even at 1.5 K. The main $k = (\frac{1}{2}, \frac{1}{2}, 0)$ type magnetic structure resembles strongly one of several possible solutions found before for La_2NiIrO_6 [30]. The coexistence of two magnetic propagation vectors had not been found before, and the magnetic structure model at low temperatures proposed in Ref. [29] for Nd_2NiIrO_6 differs strongly from our solution as far as the moment directions are concerned. Kayser *et al.* [28] proposed for the Nd compound

the presence of a $k = 0$ type magnetic structure at 1.5 K with moment values strongly varying from ours and those of Ref. [29]. The closeness of magnetic peaks created by $k = 0$ and $(\frac{1}{2}, \frac{1}{2}, 0)$ combined with insufficient statistics are at the origin of these different interpretations. The small size of the determined magnetic moment values of Ir^{4+} does not support the $J_{\text{eff}} = \frac{1}{2}$ model for the two compounds. It cannot, however, be excluded, as values $< 1\,\mu_B$ expected for the pure $J_{\text{eff}} = \frac{1}{2}$ model can be caused by hybridization and/or by distortion of the octahedral coordination of Ir.

ACKNOWLEDGMENTS

ILL is acknowledged for beam time allocation under the experiment code 5-31-2675 [41]. We would like to thank B. G. Stenning for his help in magnetic measurements, Robin Perry for his help in the sample preparation, and S. Langridge and A. Sundaresan for interesting discussions. D.T.A. would like to thank Engineering and Physical Sciences Research Council UK for funding (Grant Ref. No. EP/W00562X/1) and the Royal Society of London for Newton Advanced Fellowship funding (Ref: NAF\R1\201248).

[1] K.-I. Kobayashi, T. Kimura, H. Sawada, K. Terakura, and Y. Tokura, Nature (London) **395**, 677 (1998).

[2] D. Serrate, J. M. De Teresa, and M. R. Ibarra, J. Phys.: Condens. Matter **19**, 023201 (2007).

[3] J. M. De Teresa, D. Serrate, C. Ritter, J. Blasco, M. R. Ibarra, L. Morellon, and W. Tokarz, Phys. Rev. B **71**, 092408 (2005).

[4] C. Ritter, J. Blasco, J. M. De Teresa, D. Serrate, L. Morellon, J. Garcia, and M. R. Ibarra, Solid State Sci. **6**, 419 (2004).

[5] D. Rubi, C. Frontera, G. Herranz, J. L. Garcia Munoz, J. Fontcuberta, and C. Ritter, J. Appl. Phys. **95**, 7082 (2004).

[6] C. Frontera, D. Rubi, J. Navarro, J. L. García-Muñoz, J. Fontcuberta, and C. Ritter, Phys. Rev. B **68**, 012412 (2003).

[7] A. S. Ogale, S. B. Ogale, R. Ramesh, and T. Venkatesan, Appl. Phys. Lett. **75**, 537 (1999).

[8] J. Blasco, C. Ritter, L. Morellon, P. A. Algarabel, J. M. De Teresa, D. Serrate, J. Garcia, and M. R. Ibarra, Solid State Sci. **4**, 651 (2002).

[9] D. Serrate, J. M. De Teresa, P. A. Algarabel, J. Galibert, C. Ritter, J. Blasco, and M. R. Ibarra, Phys. Rev. B **75**, 165109 (2007).

[10] W. Westerburg, O. Lang, C. Ritter, C. Felser, W. Tremel, and G. Jakob, Solid State Commun. **122**, 201 (2002).

[11] A. T. Lee and C. A. Marianetti, Phys. Rev. B **97**, 045102 (2018).

[12] J. Zhang, W.-J. Ji, J. Xu, X.-Y. Geng, J. Zhou, Z.-B. Gu, S.-H. Yao, and S.-T. Zhang, Sci. Adv. **3**, e1701473 (2017).

[13] D. D. Maharaj, G. Sala, M. B. Stone, E. Kermarrec, C. Ritter, F. Fauth, C. A. Marjerrison, J. E. Greedan, A. Paramekanti, and B. D. Gaulin, Phys. Rev. Lett. **124**, 087206 (2020).

[14] J. Blasco, J. L. Garcia-Munoz, J. Garcia, G. Subias, J. Stankiewicz, J. A. Rodriguez-Velamazan, and C. Ritter, Phys. Rev. B **96**, 024409 (2017).

[15] A. J. Dos Santos-Garcia, C. Ritter, E. Solana-Madruga, and R. Saez-Puche, J. Phys.: Condens. Matter **25**, 206004 (2013).

[16] E. Solana-Madruga, A. J. Dos Santos-Garcia, A. M. Arevalo-Lopez, D. Avila-Brande, C. Ritter, J. P. Attfield, and R. Saez-Puche, Dalton Trans. **44**, 20441 (2015).

[17] A. M. Arevalo-Lopez, F. Stegemann, and J. P. Attfield, Chem. Comm. **52**, 5558 (2016).

[18] E. Solana-Madruga, A. M. Arevalo-Lopez, A. J. Dos Santos-Garcia, E. Urones-Garrote, D. Avila-Brande, R. Saez-Puche, and J. P. Attfield, Angew. Chem. Int. Ed. **55**, 9340 (2016).

[19] B. J. Kim, H. Jin, S. J. Moon, J. Y. Kim, B. G. Park, C. S. Leem, J. Yu, T. W. Noh, C. Kim, S. J. Oh *et al.*, Phys. Rev. Lett. **101**, 076402 (2008).

[20] X. Wan, A. M. Turner, A. Vishwanath, and S. Y. Savrasov, Phys. Rev. B **83**, 205101 (2011).

[21] J. Chaloupka, G. Jackeli, and G. Khaliullin, Phys. Rev. Lett. **105**, 027204 (2010).

[22] H. Guo, C. Ritter, and A. C. Komarek, Phys. Rev. B **94**, 161102(R) (2016).

[23] H. Guo, C. Ritter, and A. C. Komarek, Phys. Rev. B **96**, 144415 (2017).

[24] H. Zhang, K. Haule, and D. Vanderbilt, Phys. Rev. Lett. **111**, 246402 (2013).

[25] G. Cao, A. Subedi, S. Calder, J.-Q. Yan, J. Yi, Z. Gai, L. Poudel, D. J. Singh, M. D. Lumsden, A. D. Christianson *et al.*, Phys. Rev. B **87**, 155136 (2013).

[26] M. Vogl, R. Morrow, A. A. Aczel, R. B. Rodriguez, A. U. B. Wolter, S. Wurmehl, S. Aswartham, and B. Büchner, Phys. Rev. Materials **4**, 054413 (2020).

[27] H. Guo, C. Ritter, Y. Su, A. C. Komarek, and J. S. Gardner, Phys. Rev. B **103**, L060402 (2021).

[28] P. Kayser, A. Munoz, J. L. Martinez, F. Fauth, M. T. Fernandez-Diaz, and J. A. Alonso, Acta Mater. **207**, 116684 (2021).

[29] T. Ferreira, S. Calder, D. S. Parker, M. H. Upton, A. S. Sefat, and H.-C. zur Loye, Phys. Rev. Materials **5**, 064408 (2021).

[30] S. Sharma, C. Ritter, D. T. Adroja, G. B. Stenning, A. Sundaresan, and S. Langridge, Phys. Rev. Materials **6**, 014407 (2022).

[31] A. V. Powell, J. G. Gore, and P. D. Battle, J. Alloys Compd. **201**, 73 (1993).

[32] J. Rodriguez-Carvajal, Phys. B: Condens. Matter **192**, 55 (1993).

[33] K. Kobayashi, T. Nagao, and M. Ito, Acta Crystallog. A **67**, 473 (2011).

[34] J. Rodriguez-Carvajal, BASIREPS: a program for calculating irreducible representations of space groups and basis functions for axial and polar vector properties. Part of the FULLPROF Suite of programs. www.ill.eu/sites/fullprof/.

[35] C. Ritter, Solid State. Phenom. **170**, 263 (2011).

[36] M. I. Aroyo, J. M. Perez-Mato, C. Capillas, E. Kroumova, S. Ivantchev, G. Madariaga, A. Kirov, and H. Wondratschek, Z. Kristallogr. Cryst. Mater. **221**, 15 (2006).

[37] J. Mravlje, M. Aichhorn, and A. Georges, Phys. Rev. Lett. **108**, 197202 (2012).

[38] M. Moretti Sala, S. Boseggia, D. F. McMorrow, and G. Monaco, Phys. Rev. Lett. **112**, 026403 (2014).

[39] I. D. Brown and R. D. Shannon, Acta Cryst. A **29**, 266 (1973).

[40] A. A. Aczel, D. E. Bugaris, J. Yeon, C. de la Cruz, H.-C. zur Loye, and S. E. Nagler, Phys. Rev. B **88**, 014413 (2013).

[41] doi: 10.5291/ILL-DATA.5-31-2675.